Structural and optical characterization and efficacy of hydrothermal synthesized Cu and Ag doped zinc oxide nanoplate bactericides

C. Abinaya, M. Marikkannan, M. Manikandan, J. Mayandi, P. Suresh, V. Shanmugaiah, C. Ekstrum, Joshua M Pearce

Preprint: C. Abinaya, M. Marikkannan, M. Manikandan, J. Mayandi, P. Suresh, V. Shanmugaiah, C. Ekstrum, J.M. Pearce, Structural and optical characterization and efficacy of hydrothermal synthesized Cu and Ag doped zinc oxide nanoplate bactericides. *Materials Chemistry and Physics* **184** (2016), pp. 172–182. http://dx.doi.org/10.1016/j.matchemphys.2016.09.039

Structural and optical characterization and efficacy of hydrothermal synthesized Cu and Ag doped zinc oxide nanoplate bactericides

C. Abinaya [a], M. Marikkannan[a], M. Manikandan[a], J. Mayandi[a, b*], P. Suresh[c], V. Shanmugaiah[c], C. Ekstrum[b], J. M. Pearce[b, d]

[a] Department of Materials Science, School of Chemistry, Madurai Kamaraj University, Madurai- 625 021, Tamil Nadu, India.
[b] Department of Materials Science and Engineering, Michigan Technological University, Houghton - 49931 1295, Michigan, USA.
[c] Department of Microbial Technology, School of Biological Sciences, Madurai Kamaraj University, Madurai - 625 021, Tamil Nadu, India.
[d] Department of Electrical & Computer Engineering, Michigan Technological University, Houghton - 49931 1295, Michigan, USA.

*Corresponding author. Tel No.: +91 9486979772
E-mail address: jeyanthinath@yahoo.co.in (Dr. M. Jeyanthinath).

Abstract

This study reports on a novel synthesis of pure zinc oxide and both Cu and Ag doped ZnO nanoplates using a simple and low-cost hydrothermal method. The structural and optical properties of the nanoplates were quantified and the materials were tested for antibacterial activity. X-ray diffraction revealed the formation of the wurtzite phase of ZnO and scanning and transmission electron microscopy showed the formation of randomly oriented ZnO nanoplates, having thickness less than 80 nm and diameter less than 350 nm. The elemental analyses of both the pure and doped samples were evaluated by energy dispersive X-ray spectrometry. The FTIR spectra of ZnO nanomaterials showed the predictable bands at 3385 cm^{-1} (O–H stretching), 1637 cm^{-1} (stretching vibration of H_2O), 400 cm^{-1} to 570 cm^{-1} (M-O stretching). The as synthesized samples showed a strong absorption peak in the UV region (~376 nm) and a near band edge emission at 392 nm with some defect peaks in the visible region. *Escherichia coli*, *Staphylococcus aureus* and *Salmonella typhi* bacteria were used to evaluate the antibacterial activity of undoped and doped ZnO. Although all the materials showed some antibacterial characteristics, the Ag doped ZnO exhibited remarkable destruction of bacteria with low minimum inhibitory concentration (MIC) values of 40 µg/ml for *E.coli* and *S.aureus* and only 20 µg/ml (*S.typhi),* which are comparable to commercial antibiotics without optimization. Further, these chemically modified nanoparticles will be applicable for various industrial or medicinal applications such as the deposition of antimicrobial coatings and food packaging applications.

Keywords: nanostructures; oxides; chemical synthesis; electron microscopy

I. Introduction

Zinc oxide (ZnO) has attracted much attention in the scientific community as future material, which has been under study since 1935 [1]. As ZnO has a wide band gap (3.37 eV at room temperature) and large exciton binding energy (60 meV) [2] it has a variety of applications such as: transparent conducting oxides (TCOs) for solar photovoltaic (PV) devices [3,4], sophisticated back reflectors for PV [5], materials in plasmonic enhanced PV [6] and dye-sensitized PV [7-9], light emitting diodes [10,11], quantum dots [12], blue-UV optoelectronics and semiconductor spintronics [13,14]. The morphology, crystal structure, crystalline size and density of ZnO depends on the synthesis methods and dopants. ZnO is transparent to visible light and can be made highly

conductive by doping [15]. Many wet chemical methods are available for the synthesis of ZnO nano materials such as spray pyrolysis [16], hydrothermal [17-19], solvothermal [20], sol-gel [21], precipitation [22] and co precipitation [23]. The hydrothermal method is widely used as it avoids toxic and expensive solvents for the preparation of crystalline oxide materials [24]. For the preparation of oxide nanoparticles, normally three methods are involved, such as hydrolysis, oxidation and thermolysis; all performed under hydrothermal conditions [25]. The hydrothermal method is a promising method for the synthesis of high-purity materials with control over the homogeneous composition without any need for high temperature calcination processes and crushing, thus saving both energy and cost. It is relatively easy to control the purity, composition, size and the crystal shape of the powder and hence makes it possible to tailor the material for specific applications viz. disease control.

With the outbreak of infectious diseases by different pathogenic bacteria's the researchers are on a look out for new antibacterial agents. Development of new drugs is one method to combat infectious disease and nanotechnology has a greater scope in the future [26]. With the ever-increasing ineffectiveness of traditional antibiotics and developing resistance in disease organisms, a crisis is underway [27]. Nanoparticles have been receiving a warm welcome for their potential antimicrobial effects and applications [28]. The Food and Drug Administration (FDA) of the United States recognizes ZnO as one of the safest materials [29]. ZnO materials possess unique physico-chemical, optical and biological properties and it has a broad antimicrobial activity against bacteria [30], fungus [31] and virus [32]. It was reported in a previous work that ZnO particles prepared by chemical method had antibacterial properties [33]. The antibacterial mechanism of ZnO has been usually attributed to the destruction of the outer membrane of bacteria by the generation of anion radicals as a reactive element [34]. They are used in a variety of biological applications such as baby powders, barrier and calamine lotions, anti-dandruff shampoos and antiseptic creams [35]. Thus whilst ZnO already has a wide application base and antibacterial; property, it sure has the potential to be nana-engineered for a more effective disease fighter [33]. The bioactive metals such as silver, copper and zinc are becoming an alternate for the development of advanced biomaterials with antimicrobial properties. [36]

To evaluate the potential of ZnO for the above said application, Cu and Ag doped ZnO powders (Cu:ZnO and Ag:ZnO) were synthesized using low-cost simple hydrothermal method in this study. The effect of doping Cu and Ag on ZnO were studied with structural and optical characterization techniques and typical human bacterial pathogens such as *E. coli*, *S. typhi* and *S. aureus* were used to evaluate the antibacterial activity of the synthesized nanoplates. The results of the synthesized nanoplates and their impact on the ZnO ability to kill the bacteria at low concentrations are discussed below.

II. Experimental Methods

Materials

Double distilled water was used as the solvent medium in the reaction scheme, which was purchased from Borosil. Zinc acetate dihydrate, sodium hydroxide, silver nitrate and copper (II) acetate monohydrate were purchased from Merck with 98%, 97%, 99% and 98% purity respectively. All the chemicals and reagents were used without further refining.

Hydrothermal Synthesis

In the hydrothermal synthesis, 3 g of the precursor [zinc acetate dihydrate ($Zn(CH_3COO)_2 . 2H_2O$)] was dissolved in 75 ml of double distilled water and stirred for 15 minutes using a magnetic stirrer. Simultaneously, 2.4 g of NaOH was dissolved in 75 ml of double distilled water and stirred for 15 minutes. This NaOH solution was added drop wise into the aqueous zinc acetate solution

under vigorous stirring for 30 minutes at room temperature to produce a white, gelatinous precipitate.

$$Zn(CH_3COO)_2.2H_2O + 2NaOH \quad Zn(OH)_2 + 2CH_3COONa + 2H_2O \quad (1)$$

It was sealed in an autoclave and placed inside the muffle furnace at a temperature of 160ºC for 5 hours. A precipitate was formed at the bottom of the autoclave and it was allowed to cool to room temperature naturally. The obtained precipitate was centrifuged and thoroughly rinsed with distilled water and ethanol three times to remove the residual sodium salt CH_3COONa.

$$Zn(OH)_2 + 2H_2O \quad Zn(OH)_4^{2-} + 2H^+ \quad (2)$$

$$Zn(OH)_4^{2-} \quad ZnO + H_2O + 2OH^- \quad (3)$$

Finally, the product was dried at 120ºC for 1 hour using a hot plate to obtain ZnO nanopowder. A similar procedure was followed for the synthesis of Ag and Cu doped ZnO nanopowder as well, with the dopants added in the proportion of 5%. The process is summarized in Figure 1.

Methods of Characterization

A. X-ray Diffraction (XRD) Measurements

XRD was investigated for the crystalline purity of ZnO with a Bruker X-ray diffractometer (Model AXS D8 Advance using Cu Wavelength 1.5406 nm).

B. Morphological Characterizations

(i) Field Emission Scanning Electron Microscopy (FESEM)

The morphological features were recorded by FESEM (Hitachi S-4700) with an accelerating voltage of ~50kV and an elemental composition was obtained using an energy-dispersive X-ray spectrometer (FEI Philips XL).

(ii) High Resolution Transmission Electron Microscopy (HRTEM)

The morphology of the samples was examined by a Tecnai G2–TF 20 (FEI) transmission electron microscope operated at 200 kV. Samples were dispersed in ethanol and placed on the carbon coated copper grid.

The thickness and diameter of the nanoplates by FESEM and HRTEM were measured using ImageJ software (freeware available from website http://rsb.info.nih.gov/ij).

C. Spectroscopic Measurements

(i) Fourier transmission infrared (FT-IR) spectra

The FT-IR spectra of the samples was recorded on a Thermo Nicolet 6700 instrument using the KBr pellet technique in the range of 4000 cm^{-1} to 400 cm^{-1}.

(ii) UV- Vis Spectroscopic Measurements

The absorption spectrum of ZnO was obtained by dispersing ZnO powder in distilled water and using distilled water as the reference [37] with an Agilent 8453 UV-Visible spectrophotometer from 200-800 nm.

(iii) Room Temperature Photoluminescence (PL) Spectroscopy

The PL emission spectrum was obtained with Agilent spectrofluorometer carry eclipse under 325 nm excitation wavelength.

D. Antibacterial activity determination

In this experiment, the test human pathogenic bacterial cultures such as *Escherichia coli*, *Staphylococcus aureus* and *Salmonella typhi* were obtained from the Department of Microbial Technology, School of Biological Sciences, Madurai Kamaraj University, Madurai, Tamil Nadu, India and the antimicrobial activity of synthesized nanoparticles was performed by well diffusion method [38]. The human bacterial pathogens such as *Escherichia coli* (MTTC443) *Staphylococcus aureus* (MTCC3160) and *Salmonella typhi* (MTCC3216) were maintained on nutrient agar (NA):

beef extract 1.0 (g/L); yeast extract 2.0 (g/L); peptone 5.0 (g/L); NaCl 5.0 (g/L); agar 15.0 (g/L); distilled H_2O 1 L; pH 7.2 in slants or petri plates at room temperature (28 ± 2°C).

The compounds ZnO, Cu:ZnO and Ag:ZnO synthesized by hydrothermal method and it was tested for antibacterial activity by well diffusion method on Muller - Hinton Agar (MHA) medium. The effect of different nanoparticles on the growth of human pathogens and their minimal inhibitory concentration (MIC) was performed [39]. The nanoparticles with different concentration at 5 – 120 mg/ml in 10 % dimethyl sulfoxide (DMSO) was used. Tetracycline and DMSO acts as positive and negative control, respectively. The MIC value is the lowest concentration of compound that inhibited bacterial growth after incubation at 37°C for 24 h. The experiments were performed in triplicates.

III Results and Discussion

A. X- Ray Diffraction

Figure 2 shows the XRD spectra for pure ZnO, Cu and Ag doped ZnO nanoparticles synthesized using hydrothermal method. The observed diffraction peaks were in good agreement with standard data (JCPDS-89-0510); hexagonal wurtzite structure of ZnO with the space group P63mc (No.186). All samples were highly oriented along the (101) reflection plane with polycrystalline nature. The additional diffraction peak shown at 38.02° could be ascribed for face centered cubic structure of metallic Ag (*) with the space group Fm3m (No.225) (JCPDS - 04-0783) for Ag doped ZnO nanoparticles. The intensity of the Cu and Ag doped ZnO diffractions lines were decreased and a minor shift was also observed due to the substitution of Cu and Ag atoms in ZnO hexagonal lattices [40]. The crystallite size of the pure and doped samples were calculated from the Scherrer's formula [41],

$$D = \frac{K\lambda}{\beta \, Cos\theta} \qquad (4)$$

Where D is the grain size, λ is the wavelength of Cu Kα (1.5406 Å), β is the full width at half maximum (FWHM) and θ is peak position. The average crystallite sizes of the pure and doped ZnO nanoparticles were listed in the Table 1. The particle size is decreased by the foreign impurities, which can shrink the nucleation and reduce the growth rate of ZnO nanoparticles [42]. The results showed a decrease of the doped ZnO nanoparticles size from 35 nm (pure ZnO) to 28 nm for Cu:ZnO and 31 nm for Ag: ZnO samples, respectively. The FWHM of the Cu and Ag doped samples were increased, compared to the pure ZnO. Zeferino et al. proposed that the intensity of Ag doped ZnO diffraction lines were decreased and the FWHM increases with the incorporation Ag in the ZnO lattices [43]. From the diffraction results, the observed lattice parameters are in good agreement with the reported values and small changes in lattice constants were caused by the occupation of Cu and Ag atoms in the ZnO lattice with the formation of complex defects [44]. The difference in ionic radius may influence the lattice parameters of the doped ZnO nanoparticles. The volume of the unit cell was estimated using the formula and listed in Table 1. The values for Cu and Ag doped ZnO nanoparticles were greater when compared to the pure ZnO. According to the Vegard's law, the unit cell volume has increased with the higher doping levels [45]. The Ag doped ZnO nanoparticles have attained the highest volume (48.01 $Å^3$) due to the ionic radius of Ag^{2+} (1.22 Å) and Zn^{2+} (0.74 Å).

B. Morphological Investigation

(i) Field Emission Scanning Electron Microscopy

The morphological features of ZnO along with doped samples such as Cu:ZnO and Ag:ZnO are shown in Figure 3(a-c) respectively. In general, the surface morphology is greatly influenced by

sample preparation and addition of external impurities. The images for all three materials reveal the morphology as nanoplates. Although the size of the nanoplates was inhomogeneous, they distributed with a definite form and grain boundary, apparently with no porosity. They are determined to be densely packed, randomly oriented. The thickness of nanoplates ranges from 60 nm to 80 nm and diameters from 250 nm to 350 nm [46]. Here the surface morphology has not changed by dopants. A careful observation of the SEM images shows that for pure ZnO samples the nanoplates were uniformly distributed, but in the case of doped samples, there was a slight change in the distribution. In the pure ZnO, all the plates were almost in the same size, but for the Ag and Cu doped ZnO a greater diversity of size with some small and some larger plates are present. Because of this it appears as if the distribution is loosely or densely packed.

EDX-Elemental composition: The elemental composition of the samples such as Zn, Cu, Ag and O were examined using EDX and the spectra of pure ZnO, Cu:ZnO and Ag:ZnO are shown in Figure 4(a-c). The estimation of the quantitative weight and atomic percentage of the as synthesized samples was presented in inset of Figure 4. The presence of carbon is due to the carbon grid. EDX confirms the presence of Cu and Ag in ZnO. The absence of any other peak except those due to the components in the samples is the evidence for the quality of samples without any elemental impurities. For doped samples a reduction in crystalline quality of ZnO particles has been observed in XRD, which is due to the decrease in zinc concentration [Pure ZnO (78.45%) > Ag:ZnO (68.47%) >Cu:ZnO (66.70%)]. In case of oxygen concentration Cu:ZnO has the highest weight % as 27.52% than pure ZnO (20.18%) and Ag:ZnO (23.66%). The optimal wt.% of zinc and oxygen plays a substantial part in the destruction of cell walls.

(ii) High Resolution Transmission Electron Microscopy

Figure 5 shows the HRTEM images of ZnO (a, d), Cu:ZnO (b, e) and Ag:ZnO (c, f) and inset shows the SAED patterns (g, h & i) respectively. As seen, the images confirms the formation of nanoplates. The diameter and thickness of all the samples were around 250-350 nm and 60-80 nm. It is consistent with SEM results. The lattice fringes with an interplanar spacing (d) of ~0.25 nm corresponds to the (101) crystal plane of ZnO nanoplates. Electron diffraction (ED) performed on a selected area (Inset of Figure 5 (g, h, i)) confirms the presence of planes such as {(101), (002), (101), (102)}, which corresponds to the hexagonal (wurtzite ZnO) P63mc structure. These planes and the d spacing measured from HRTEM were consistent with the XRD analysis.

Spectroscopic Analysis

(i) FT-IR Spectra

Infrared spectroscopic analysis is used to analyze the vibration bands due to Zn-O bound, the changes due to Cu and Ag substitution and hydrogen bonding. Typical infrared transmittance spectra of pure and doped ZnO samples synthesized by hydrothermal method are displayed in Figure 6. The peaks appearing between 400 cm^{-1} to 550 cm^{-1} were assigned to the meta-oxygen (M-O) stretching mode [47 48, 49]. At the same time a broad absorption band at 3438 cm^{-1} can be observed that corresponds to the O–H stretching vibration of water molecule adsorbed on the surface [50]. The band at 1638 cm^{-1} can be associated with the stretching vibration of H_2O molecules [51]. The band appearing at 880 cm^{-1} was due to the presence of stretching and bending vibrations of C-O species [52].

The FT-IR spectra of Ag and Cu doped ZnO shows the presence of new peaks at 1379 and 1427 cm^{-1} when compared to pure ZnO [53, 54]. This may be due to the symmetric and asymmetric stretching bands of acetate species from precursors [55, 56]. As the size of nanoparticles increases, there will be decreased carboxylate COO- and hydroxyl group –OH [57]. The source of these peaks remains

the same as explained above, due to similar reaction environment for all the undoped and doped samples.

(ii) UV-Vis Spectral Analysis

The UV-visible absorption spectra of the as-synthesized pure ZnO and Cu, Ag doped ZnO samples are depicted in Figure 7. All the samples have a strong absorption maximum below 400 nm. The strong absorption in the UV region reveals that the absorption band of ZnO nanoparticles was ascribed to the intrinsic transition between the valence band (VB) and the conduction band (CB) [58]. The result shows that the UV absorption peak for undoped ZnO was observed around 377 nm. For Cu: ZnO, absorption at 375 nm confirms that the spectrum was slightly blue shifted due to the quantum confinement effect and Ag: ZnO was slightly red shifted(~380)with a decreased band gap that was evidenced by shifting of the absorption peak towards higher wavelength [59]. The red shifted absorption edge for the Ag:ZnO suggests that more absorption states or defect energy bands exist in the sample, which may be related to the specific hydrothermal condition in the synthesis of ZnO.

(iii) Photoluminescence Spectroscopy

Figure 8 shows the room temperature PL spectra of the pure and Cu, Ag doped ZnO nanoparticles as-synthesized by hydrothermal method. All the samples have similar emission peaks centered at 392, 403, 419, 444, 460, 486, 496 and 520 nm. In general, the PL spectra of ZnO nanoparticles usually have two emission bands. One is in the UV region, which is attributed to the near-band-edge emission through exciton–exciton collision processes. The other is in the visible region, due to electron–hole recombination caused by intrinsic point defects and surface defects (e.g., oxygen vacancies, zinc interstitials, and the incorporation of hydroxyl groups) in the crystal lattice during solution growth [60]. The peak at 392 nm in as-synthesized pure ZnO may be attributed to near band edge emission [61] and the peak after 403 nm was originated due to defect states. The emission at 419 nm was associated with an electron transition from a shallow donor level of neutral zinc interstitial to the top level of the valence band. The emission at 444 and 486 nm is ascribed to surface defects of ZnO. The green emission at 520 nm may be assigned to oxygen vacancies [62].The peaks centered at 392 nm, 419 nm (violet emission) and 496 nm were Donor Level (DL) sub peaks and the peaks centered at 460 nm (blue emission), 522 nm (green emission) were Acceptor Level (AL sub peaks) [63]. The asymmetric spectra are due to the native defect states of ZnO [64]. The probability of the contribution of these defects states with luminescence increases when ZnO was sized in nano dimension. Therefore, size, morphology, surface roughness and external doping to ZnO [65] can control these defect emissions. Thus, the defects due to native oxygen vacancies were responsible for the visible emissions in ZnO samples. However, some controversy in assigning the defect emissions in ZnO [66].

D. Antimicrobial Assays

The hydrothermally synthesized pure and doped ZnO samples exhibited antibacterial activity against tested human pathogenic bacteria at different concentrations. Dose dependent activity was observed on the synthesized nanoparticle and it was found to be significant even at lowest concentration. The difference between gram positive and gram-negative bacteria are normally reported in the literature [67]. The difference in activity against these two types of bacteria can be explained by the different structures and chemical compositions of the cell wall. The cell wall of gram-negative bacteria was different from that of the gram-positive bacteria by having an outer lipopolysaccharide (LPS) membrane that covers the peptidoglycan layer [68]. It also helps the bacteria to survive in situations where the presence of external substances that can harm it. There are two possibilities for the de-

struction of bacterial cell. The obtained reactive oxygen species such as •OH and $•O^{2-}$ can induce oxidative degradation of lipids in membranes that leads to DNA damage [69]. Another mechanism is the inhibition of bacterial cells by interaction between positively charged ZnO with the negatively charged bacterial cell wall.

The results showed that ZnO nanoparticles exhibited bactericidal effects in dark conditions. After incubation under appropriate condition, the MIC value of the sample was obtained as 20 to 120 µg/ml. The nanoparticle Ag:ZnO showed remarkable antibacterial activity against tested panel of pathogens namely, *E. coli* (MTTC443) *S. aureus* (MTCC3160) and *S. typhi* (MTCC3216) compared to a commercial antibiotic and control (DMSO). Figure 9 shows the MIC values for undoped ZnO, Cu:ZnO and Ag:ZnO against *E. coli*, *S. aureus* and *S. typhi*. Tetracycline has the lowest concentration ranging from 10 to 40 µg/ml for all tested three pathogens. Ag:ZnO, Cu:ZnO and ZnO showed significant antibacterial activity of the above mention bacterial pathogens ranging from 20-40 µg/ml, 50-70 µg/ml and 80-100 µg/ml respectively.

Because of the potent interaction between metallic Ag and the semiconductor ZnO, this synergistic Ag:ZnO showed enhanced antibacterial activities for both gram-negative and gram-positive bacteria. This metallic interaction was due to ionic radii mismatch between Ag^{2+} (1.22 Å) and Zn^{2+} (0.74 Å) but the ionic radii of Cu^{2+} is 0.73 Å. Ag: ZnO nanoplates have the smallest crystallite size, positive surface charge (which results in the nanoparticle being drawn to the negatively charged surface of the bacteria), high surface area ratio and narrowest size distribution, generally enhances a bactericidal effect [70].

The increasing bacterial resistance to commercial antibiotics leads to the investigation on the antibacterial activity of silver nanoparticles [70]. From the literature survey it has been demonstrated that silver is non-toxic to human cells at lower concentration [71, 30]. Silver species release Ag+ ions and they interact with the thiol groups in bacteria proteins, affecting the replication of DNA [72]. Comparing with pure silver nanoparticles Ag doped ZnO have many advantages such as low toxicity and cost effective. The inhibitory concentration of the Ag:ZnO nanoparticle was found to be similar to that of the MIC value of the approved antibiotics [73]. To the best of our knowledge, these are the lowest MIC value reported for all the samples particularly for silver doped ZnO. The reason for the appearance of remarkable antimicrobial activities may principally originate from the presence of both Ag and ZnO nanoparticles. It is also reported that the chemical modifications on a nanoparticle's surface alter its interactions with biological systems [74].

It is clearly warranted that the optimization of doped ZnO synthesis method, will lead to increase the efficacy against multidrug resistant bacteria such as methicillin-resistant *Staphylococcus aureus* (MRSA), vancomycin-resistant *Enterococcus* (VRE) and multi-drug-resistant (MDR) *Mycobacterium tuberculosis* (MDR-TB) [75]. These pathogens have mutated in such a way they cannot be controlled or killed by antibiotics, however, these same mutations are not relevant to doped ZnO-based bactericides. In future, clinical trials can be carried out using the optimized Ag doped ZnO to overcome the resistance of MDR bacteria to avoid growing global public health problems.

IV. Conclusions

To summarize, ZnO nanoplates have been successfully synthesized with a low temperature and aqueous solution-based method without a calcination process. This method was also found to be easy and simple approach for the incorporation of Cu and Ag dopants into ZnO. XRD results confirmed that the synthesized samples were in hexagonal wurtzite structure. From the FESEM images it is observed that although the morphology does not change with dopants it has increased antibacterial activity compared to pure ZnO. HRTEM results also confirmed the morphology as nanoplates. The absence of impurities and the presence of Cu and Ag were evidenced by EDX. The absorption edge falls under the UV region and the emission peaks were associated with several

intrinsic defects such as V_O, V_{Zn}, O_i, etc., with the decreased intensity for doped samples. The most interesting observation was found that the Ag doped ZnO has MIC values against *E.coli, S.aureus and S.typhi* comparable to commercial antibiotics, which has the mechanism for bactericide. It represents a major potential benefit in the battle against anti-biotic resistant pathogens for a large number of medical and health applications. The results suggest that Ag:ZnO synthesized with this low-cost industrially-scalable process has significant potential as an antimicrobial agent against both gram positive and gram negative bacteria. This result is considered as an influential application forecast and it has marketable significance. Further standardization may be able to enhance the clinical effects against resistant pathogenic bacteria's.

Acknowledgments

AC thanks the DST-INSPIRE New Delhi, India for the financial assistance as fellowship. JM, thanks the DST-SERB for the partial support through the project SERB/F/1829/2012-13 and thank UGC, New Delhi, INDIA for providing support through RAMAN fellowship 2014-2015 to visit Michigan Technological University, USA. The authors would like to acknowledge helpful comments from J. Bow. We thank UPE-MKU for providing TEM facilities.

References

1. C. W. Bunn, A Comparative Review of ZnO Materials and Devices, Proc. Phys. Soc. London 47 (1935) 835.
2. M. Li, H. Bala, X. Lv, X. Ma, F. Sun, L. Tang, Z. Wang, Direct synthesis of monodispersed ZnO nanoparticles in an aqueous solution, Mater. Lett. 61 (2007) 690-693.
3. K. Iwata, T. Sakemi, A. Yamada, P. Fons, K. Awai, T. Yamamoto, S. Shirakata, K. Matsubara, H. Tampo, K. Sakurai, S. Ishizuka, S. Niki, Improvement of ZnO TCO film growth for photovoltaic devices by reactive plasma deposition (RPD), Thin Solid Films 480 (2005) 199-203.
4. E. Fortunato, D. Ginley, H. Hosono, D. C Paine, Transparent conducting oxides for photovoltaics, MRS Bull. 32 (2007) 242-247.
5. S. Y. Myong, K. S. Lim, J. M. Pearce, Double amorphous silicon-carbide p-layer structures producing highly stabilized pin-type protocrystalline silicon multilayer solar cells, Appl. Phys. Lett. 87 (2005) 193509.
6. G. Jephias, A. Vora, R. R. Khanal, A. B. Phillips, M. J. Heben, D. O. Guney, P. Bergstrom, A. Kulkarni, J. M. Pearce, Limitations of ultra-thin transparent conducting oxides for integration into plasmonic-enhanced thin-film solar photovoltaic devices, Mater. Renewable Sustainable Energy 4 (2015) 1-12.
7. M. Grätzel, Solar Energy Conversion by Dye-Sensitized Photovoltaic Cells, Inorg. Chem. 44 (2005) 6841-6851.
8. A. B. Martinson., J. W. Elam, J. T. Hupp, M. J. Pellin, ZnO Nanotube Dye-Sensitized Solar Cells, Nano Lett. 7 (2007) 2183-2187.
9. M. Prabhu, J. Mayandi, R. N. Mariammal, V. Vishnukanthan, J. M. Pearce, N. Soundararajan, K. Ramachandran, Peanut shaped ZnO microstructures: controlled synthesis and nucleation growth toward low-cost dye sensitized solar cells, Mater. Res. Express 2 (2015) 066202.
10. J. H. Lim, C. K. Kang, K. K. Kim, I. K. Park, D. K. Hwang, S. J. Park, UV Electroluminescence Emission from ZnO Light-Emitting Diodes Grown by High-Temperature Radiofrequency Sputtering, Adv. Mater. 18 (2006) 2720-2724.
11. S. J. Jiao, Z. Z. Zhang, Y. M. Lu, D. Z. Shen, B. Yao, J. Y. Zhang, Z. K. Tang, ZnO p-n junction light-emitting diodes fabricated on sapphire substrates, Appl. Phys. Lett. 88 (2006) 031911-031914.
12. S. Mahamuni, K. Borgohain, B. S. Bendre, V. J. Leppert, S. H. Risbud, Spectroscopic and structural characterization of electrochemically grown ZnO quantum dots, J. Appl. Phys. 85 (1999) 2861-2865.

13. C. Klingshirn, ZnO: From basics towards application, Phys. Status Solidi B 244 (2007) 3027-3073.
14. U. Ozgur, Y. I. Alivov, C. Liu, A. Teke, M. A. Reschchikov, S. Dogan, V. Avrutin, S. J. Cho, H. Morkoc, A comprehensive review of ZnO materials and devices, J. Appl. Phys. 98 (2005) 0410301.
15. D. Raoufi, T. Raoufi, The effect of heat treatment on the physical properties of sol–gel derived ZnO thin films, Appl. Surf. Sci. 255 (2009) 5812-5817.
16. S. B. Zhang, S. H. Wei, A. Zunger, Intrinsic n-type versus p-type doping asymmetry and the defect physics of ZnO, Phys. Rev. B 63 (2001) 075 205.
17. D. Polsongkram, P. Chamninok, S. Pukird, L. Chow, O. Lupan, G. Chai, H. Khallaf, S. Park, A. Schulte, Effect of synthesis conditions on the growth of ZnO nanorods via hydrothermal method, Physica B 403 (2008) 3713-3717.
18. C. X. Xu, A. Wei, X. W. Sun, Z. L. Dong, Aligned ZnO nanorods synthesized by a simple hydrothermal reaction, J. Phys. D: App. Phys. 39 (2006) 1690-1693.
19. J. Song, S. Baek, S. Lim, Effect of hydrothermal reaction conditions on the optical properties of ZnO Nanorods, Phys. B: Condens. Matter 403 (2008) 1960-1963.
20. J. Zhang, L. D. Sun, J. L. Yin, H .L. Su, C. S. Liao, C. H. Yan, Control of ZnO morphology via a simple solution route, Chem. Mater. 14 (2002) 4172-4177.
21. L. Spanhel, M. A. Anderson, Semiconductor clusters in the sol-gel process: quantized aggregation, gelation, and crystal growth in concentrated zinc oxide colloids, J. Am. Chem. Soc. 113 (1991) 2826-2833.
22. P. Amornpitoksuk, S. Suwanboon, S. Sangkanu, A. Sukhoom, N. Muensit, J. Baltrusaitis, Synthesis, characterization, photocatalytic and antibacterial activities of Ag-doped ZnO powders modified with a diblock copolymer, Powder Technol. 219 (2012) 158-164.
23. M. Ashokkumar, S. Muthukumaran, Microstructure, optical and FTIR studies of Ni, Cu co-doped ZnO nanoparticles by co-precipitation method, Opt Mater. 37 (2014) 671-678.
24. S. Ameen, M. S. Akhtar, H. K. Seo, Y .S. Kim, H. S. Shin, Influence of Sn doping on ZnO nanostructures from nanoparticles to spindle shape and their photoelectrochemical properties for dye sensitized solar cells, Chem. Eng. J. 187 (2012) 351-356.
25. The Chemistry of Nanomaterials: Synthesis, Properties and Applications (volume 2), edited by C. N. R. Rao, A. Muller, A. K. Cheetham, Wiley-VCH Verlag GmbH& Co.KGaA
26. K. Bourzac, Nanotechnology: Carrying drugs, Nature 491 (2012) 58-60.
27. H. C. Neu, The crisis in antibiotic resistance, Science 257 (1992) 1064-1073.
28. D. Mandal, M. E. Bolander, D. Mukhopadhyay, G. Sarkar, P. Mukherjee, The use of microorganisms for the formation of metal nanoparticles and their application, Appl. Microbiol. Biotechnol. 69 (2006) 485-492.
29.FDA,2011,http://ecfr.gpoaccess.gov/cgi/t/text/textidx?c=ecfr&sid=786bafc6f6343634fbf79fcdca7061e1&rgn=div5&view=text&node=21:3.0.1.1.13&idno=21#21:3.0.1.1.13.9.
30. L. Zhang, Y. Jiang, Y. Ding, M. Povey, D. York, Investigation into the antibacterial behaviour of suspensions of ZnO nanoparticles (ZnO nanofluids), J. Nanopart. Res. 9 (2007) 479-489.
31. A. Lipovsky, Y. Nitzan, A. Gedanken, R. Lubart, Antifungal activity of ZnO nanoparticles—the role of ROS mediated cell injury, Nanotechnology 22 (2011) 105101-105106.
32. J. You, Y. Zhang, Z. Hu, Bacteria and bacteriophage inactivation by silver and zinc oxide nanoparticles, Colloids Surf. B 85 (2011) 161-167.
33. K. R. Raghupathi, R.T. Koodali, A. C. Manna, Size-Dependent Bacterial Growth Inhibition and Mechanism of Antibacterial Activity of Zinc Oxide Nanoparticles, Langmuir 27 (2011) 4020-4028.

34. U. Sirimahachai, S. Phongpaichit, S. Wongnawa, Evaluation of bactericidal activity of TiO_2 photocatalysts: a comparative study of laboratory-made and commercial TiO_2 samples, Songklanakarin Journal of Science and Technology 31 (2009) 517-525.
35. O. Akhavan, E. Ghaderi, Enhancement of antibacterial properties of Ag nanorods by electric field, Sci Technol Adv. Mater. 10 (2009) 015003-015007.
36. F. Paladini, M. Pollini, A. Sannino, L. Ambrosio, Metal-Based Antibacterial Substrates for Biomedical Applications, Biomacromolecules 16 (2015) 1873-1885.
37. R. Kripal, A. K. Gupta, S. K. Mishra, R. K. Srivastava, A. C. Pandey, S. G. Prakash, Photoluminescence and Photocon-ductivity of ZnS:Mn^{2+} Nanoparticles Synthetized via Co-Precipitation Method, Spectrochim. Acta A. 76 (2010) 523-530.
38. Z. E. Karvani, P. Chehrazi, Antibacterial activity of ZnO nanoparticle on grampositive and gram-negative bacteria, Afr. J. Microbiol. Res. 5 (2011) 1368-1373.
39. V. Shanmugaiah, H. Harikrishnan, N. S. AlHarbi, K. Shine, J. M. Khaled,
N. Balasubramanian, G. Shyamkumar, Facile synthesis of silver nanoparticles using Streptomyces Sp.vsmgt1014 and their antimicrobial efficiency, Dig. J. Nanomater. Bios. 10 (2015) 179-187.
40. Z. Zhang, J. B. Yi, J. Ding, L. M. Wong, H. L. Seng, S. J. Wang, J. G. Tao, G. P. Li, G. Z. Xing, T. C. Sum, C. H. A. Huan, T. Wu, Cu-Doped ZnO Nanoneedles and Nanonails: Morphological Evolution and Physical Properties, J. Phys. Chem. C 112 (2008) 9579-9585.
41. M. Marikkannan, V. Vishnukanthan, A. Vijayshankar, J. Mayandi, J. M. Pearce, A novel synthesis of tin oxide thin films by the sol-gel process for optoelectronic Applications, AIP adv. 5 (2015) 027122-027130.
42. N. T. K. Thanh, N. Maclean, S. Mahiddine, Mechanisms of Nucleation and Growth of Nanoparticles in Solution, Chem. Rev. 114 (2014) 7610-7630.
43. R. S. Zeferino, M. B. Flores, U. Pal, Photoluminescence and Raman Scattering in Ag-doped ZnO Nanoparticles, J. Appl. Phys. 109 (2011) 014308-014314.
44. L. Chow, O. Lupan, G. Chai, H. Khallaf, L. K. Ono, B. Roldan Cuenya, I. M. Tiginyanuf, V. V. Ursaki, V. Sontea, A. Schulte, Synthesis and characterization of Cu-doped ZnO one-dimensional structures for miniaturized sensor applications with faster response, Sens. Actuators A 189 (2013) 399-408.
45. V. Gandhi, R. Ganesan, H. H. A. Syedahamed, M. Thaiyan, Effect of Cobalt Doping on Structural, Optical, and Magnetic Properties of ZnO Nanoparticles Synthesized by Coprecipitation Method, J. Phys. Chem. C 118 (2014) 9715-9725.
46. http://imagej.nih.gov/ij/docs/pdfs/ImageJ.pdf
47. K. Raja, P. S. Ramesh, D. Geetha, Synthesis, structural and optical properties of ZnO and Ni-doped ZnO hexagonal nanorods by Co-precipitation method, Spectrochimica Acta Part A: Molecular and Biomolecular Spectroscopy 120 (2014) 19-24.
48. S. Muthukumaran, R. Gopalakrishnan, Structural, FTIR and photoluminescence studies of Cu doped ZnO nanopowders by co-precipitation method, Optical Materials 34 (2012) 1946–1953
49. S. M. Hosseini, I. A. Sarsari, P. Kameli, and H. Salamati, Effect of Ag doping on structural, optical, and photocatalytic properties of ZnO nanoparticles, Journal of Alloys and Compounds 640 (2015) 408–415
50. S. Bagheri, K. G. Chandrappa, S. B. A. Hamid, Facile synthesis of nano-sized ZnO by direct precipitation method, Der. Pharma. Chemica 5 (2013) 265-270.
51. N. R. Yogamalar, A. C. Bose, Tuning the aspect ratio of hydrothermally grown ZnO by choice of precursor, J. Solid state chem. 184 (2011) 12-20.
52. C. P. Sibu, S. R. Kumar, P. Mukundan, K. G. K. Warrier, Structural Modifications and Associated Properties of Lanthanum Oxide Doped Sol−Gel Nanosized Titanium Oxide, Chem. Mater. 14 (2002) 2876-2881.

53. T. S. Vijayakumar, S. Karthikeyeni, S. Vasanth, A. Ganesh, G. Bupesh, R. Ramesh, M. Manimegalai, and P. Subramanian, Synthesis of Silver-Doped Zinc Oxide Nanocomposite by Pulse Mode Ultrasonication and Its Characterization Studies, Journal of Nanoscience Article ID 785064 (2013) 1-7
54. M. Ashokkumar, S. Muthukumaran, Microstructure, optical and FTIR studies of Ni, Cu co-doped ZnO nanoparticles by co-precipitation method, Optical Materials 37 (2014) 671–678
55. S. Maensiri; P. Laokul, S. Phokha, A Simple Synthesis and Magnetic Behavior of Nanocrystalline Zn0.9Co0.1O Powders by Using Zn and Co Acetates and Polyvinyl Pyrrolidone as Precursors, J. Magn. Magn. Mater. 305 (2006) 381-387.
56. G. Xiong, U. Pal, J. G. Serrano, K. B. Ucer, R. T. Williams, Photoluminesence and FTIR study of ZnO nanoparticles: the impurity and defect perspective, Phys. stat. sol. C 3 (2006) 3577-3581.
57. P. Pandey, R. Kurchania, F. Z. Haque, Controlled hydrothermal synthesis, structural and optical analysis of nanometer-sized ZnO spheres, Optik 126 (2015) 301-303.
58. M. Haase, H. Weller, A. Henglein, Photochemistry and radiation chemistry of colloidal semiconductors 23. Electron storage on zinc oxide particles and size quantization, J. Phys. Chem. 92 (1988) 482-487.
59. E. Burstein, Anomalous Optical Absorption Limit in InSb, Phys. Rev. 93 (1954) 632-633.
60. K. H. Tam, C. K. Cheung, Y. H. Leung, A. B. Djurišić, C. C. Ling, C. D. Beling , S. Fung, W. M. Kwok, W. K. Chan, D. L. Phillips, L. Ding, W. K. Ge, Defects in ZnO nanorods prepared by a hydrothermal method, J. Phys. Chem. B. 110 (2006) 20865-20871.
61. K. Prabakar, S. Venkatachalam, Y. L. Jeyachandran, S. K. Narayandass, D. Man-galaraj, Microstructure, Raman and optical studies on Cd0.6Zn0.4Te thin films, Mater. Sci. Eng. B 107 (2004) 99-105.
62. M. A. Gondal, Q. A. Drmosh, Z. H. yamani, T. A. Saleh, Synthesis of ZnO_2 nanoparticles by laser ablation in liquid and their annealing transformation into ZnO nanoparticles, Appl. Surface. Sci. 256 (2009) 298-304.
63. S. K. Mishra, S. Bayan, R. Shankar, P. Chakraborty, R. K Srivastava, Efficient UV photosensitive and photoluminescence properties of sol–gel derived Sn doped ZnO nanostructures, Sensor Actuat. A 211 (2014) 8-14.
64. N. R. Panda, D. Sahu, B. S. Acharya, P. Nayak, High UV absorption efficiency of nanocrystalline ZnO synthesized by ultrasound assisted wet chemical method, Current Appl. Phys. 15 (2015) 389-396.
65. U. Ozgür, Y. I. Alivov, C. Liu, A. Teke, M. A. Reshchikov, S. Dogan, V. Avrutin, S. J. Cho, H. Morkoc, A comprehensive review of ZnO materials and devices, J. Appl. Phys. 98 (2005) 041301-041404.
66. H. Zeng, G. Duan, Y. Li, S. Yang, X. Xu, W. Cai, Blue Luminescence of ZnO Nanoparticles Based on Non-Equilibrium Processes: Defect Origins and Emission Controls, Adv. Funct. Mater. 20 (2010) 561-572.
67. P. Amornpitoksuk, S. Suwanboon, S. Sangkanu, A. Sukhoom, J. Wudtipan , K. Srijan, S. Kaewtaro, Synthesis, characterization, photocatalytic and antibacterial activities of Ag-doped ZnO powders modified with a diblock copolymer, Powder Technol. 219 (2012) 158-164.
68. M. Fang, J. H. Chen, X. L. Xu, P. H. Yang, H. F. Hildebrand, Antibacterial activities of inorganic agents on six bacteria associated with oral infections by two susceptibility tests, Int. J. Antimicrob. Agents 27 (2006) 513-517.
69. N. Padmavathy, R. Vijayaraghavan, Enhanced bioactivity of ZnO nanoparticles-an antimicrobial study, Science and Technology of Adv. Mat. 9 (2008) 03500466.
70. A. Panacek, L. Kvitek, R. Prucek, M. Kolar, R. Vecerova, N. Pizurova, V. Sharma, T. Nevecna, R. Zboril, Silver colloid nanoparticles: synthesis, characterization, and their antibacterial activity, J. Phys. Chem. B 110 (2006) 16248-16253.

71. S. Pal, Y. K. Tak, J. M. Song, Does the Antibacterial Activity of Silver Nanoparticles Depend on the Shape of the Nanoparticle? A Study of the Gram-Negative Bacterium Escherichia coli, J. Appl. Environ. Microbiol. 73 (2007) 1712-1720.
72. M. Marini, N. Niederhausern, R. I. Seppi, M. Bondi, C. Sobia, M. Toseli, F. Pilati, Antibacterial activity of plastics coated with silver doped organic – inorganic hybrid coatings prepared by sol-gel processes, Biomacromolecules 8 (2007) 1246-1254.
73. http://www.antimicrobe.org/b237tabrev.htm
74. Q. Mu, G. Jiang, L. Chen, H. Zhou, D. Fourches, A. Tropsha, B. Yan, Chemical Basis of Interactions Between Engineered Nanoparticles and Biological Systems, Chem. Rev. 114 (2014) 7740-7781.
75. L. Pray, Gleevec: the Breakthrough in Cancer Treatment, Nature Education 1 (2008) 37.

Table Captions:

Table 1: Calculated XRD parameters for the as synthesized pure ZnO, Cu:ZnO and Ag:ZnO.

Table 2: Comparison table for the d spacing from XRD and HRTEM and size parameters calculated from FESEM and HRTEM

Figure Captions:

Figure 1. Flow Chart for the hydrothermal synthesis of pure ZnO, Cu:ZnO and Ag:ZnO

Figure 2: XRD Patterns of pure ZnO, Cu:ZnO and Ag:ZnO

Figure 3: FESEM images of the as synthesized a) pure ZnO b) Cu:ZnO c) Ag:ZnO

Figure 4: EDS results of a) pure ZnO b) Cu:ZnO c) Ag:ZnO

Figure 5: HRTEM images of the as synthesized a) pure ZnO b) Cu:ZnO c) Ag:ZnO and their respective fringe patterns (d, e and f). The inset shows the SAED patterns (g, h and i).

Figure 6: FTIR spectra of the pure ZnO, Cu:ZnO and Ag:ZnO

Figure 7: UV-Visible absorption spectra of pure ZnO, Cu:ZnO and Ag:ZnO

Figure 8: Room temperature PL spectra of pure ZnO, Cu:ZnO and Ag:ZnO

Figure 9: MIC values for pure ZnO, Cu:ZnO and Ag:ZnO against *E. coli*, *S. aureus* and *S. typhi* with tetracycline (positive control) and DMSO (negative control).

Preprint: C. Abinaya, M. Marikkannan, M. Manikandan, J. Mayandi, P. Suresh, V. Shanmugaiah, C. Ekstrum, J.M. Pearce, Structural and optical characterization and efficacy of hydrothermal synthesized Cu and Ag doped zinc oxide nanoplate bactericides. *Materials Chemistry and Physics* **184** (2016), pp. 172–182. http://dx.doi.org/10.1016/j.matchemphys.2016.09.039

Sample	d spacing (Å)	Lattice Parameters (Å)		c/a ratio	Volume (Å^3)	Grain Size (nm)	Space group
		a	b				
Pure ZnO	2.6091	3.2543	5.2183	1.6035	47.85	35	P63mc (No.186)
Cu:ZnO	2.6099	3.2554	5.2199	1.6034	47.91	28	P63mc (No.186)
Ag:ZnO	2.6110	3.2579	5.2220	1.6028	48.01	31	P63mc (No.186) and Fm3m (No.225)

Table 1

Sample	d spacing (nm)		SEM (nm)		TEM (nm)	
	XRD	TEM	Average Thickness	Diameter	Average Thickness	Diameter
Pure ZnO	0.260	0.252	70-80	250-300	50-80	100-250
Cu:ZnO	0.260	0.234	80-100	300-350	60-80	250-350
Ag:ZnO	0.261	0.236	80-90	200-250	70-80	180-220

Table 2

Preprint: C. Abinaya, M. Marikkannan, M. Manikandan, J. Mayandi, P. Suresh, V. Shanmugaiah, C. Ekstrum, J.M. Pearce, Structural and optical characterization and efficacy of hydrothermal synthesized Cu and Ag doped zinc oxide nanoplate bactericides. *Materials Chemistry and Physics* **184** (2016), pp. 172–182. http://dx.doi.org/10.1016/j.matchemphys.2016.09.039

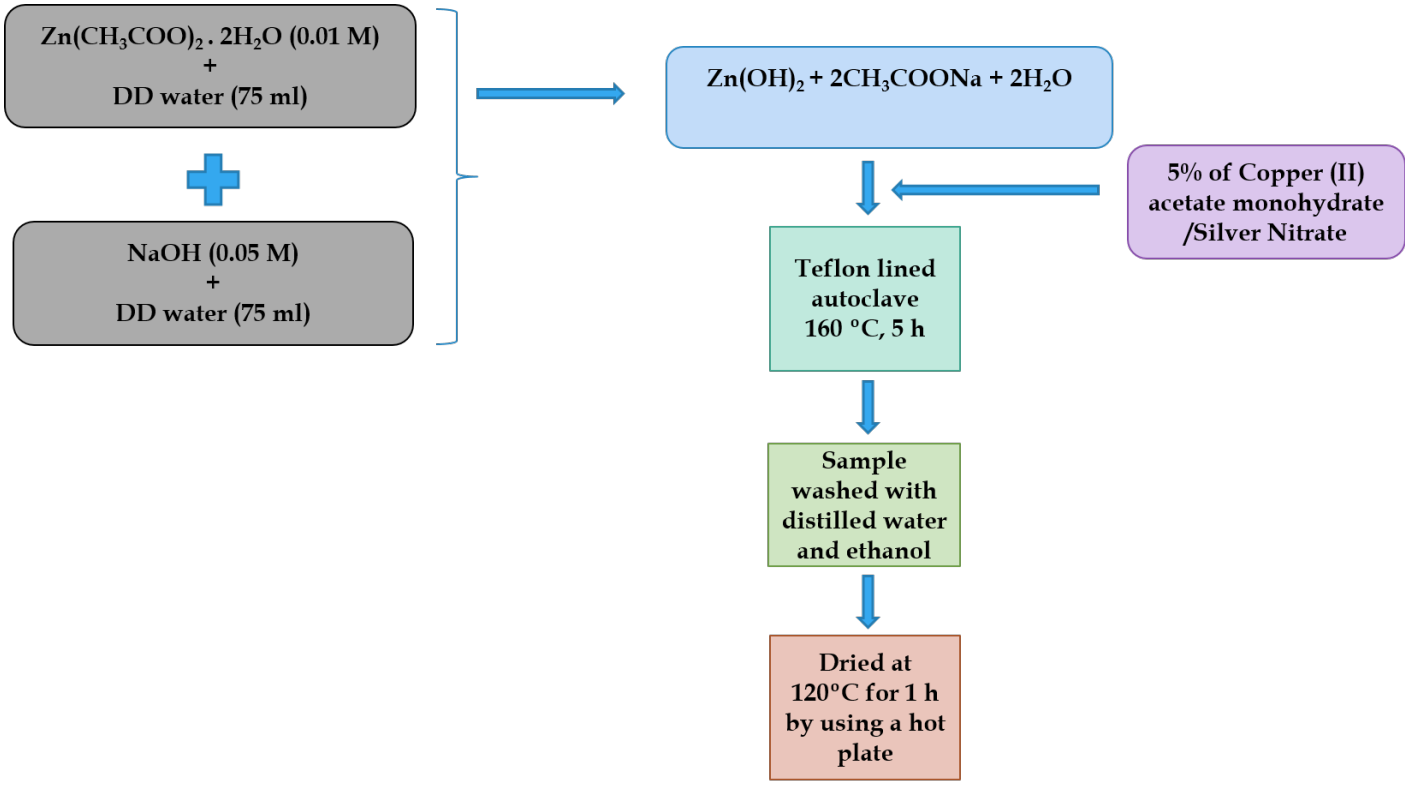

Figure 1

Preprint: C. Abinaya, M. Marikkannan, M. Manikandan, J. Mayandi, P. Suresh, V. Shanmugaiah, C. Ekstrum, J.M. Pearce, Structural and optical characterization and efficacy of hydrothermal synthesized Cu and Ag doped zinc oxide nanoplate bactericides. *Materials Chemistry and Physics* **184** (2016), pp. 172–182. http://dx.doi.org/10.1016/j.matchemphys.2016.09.039

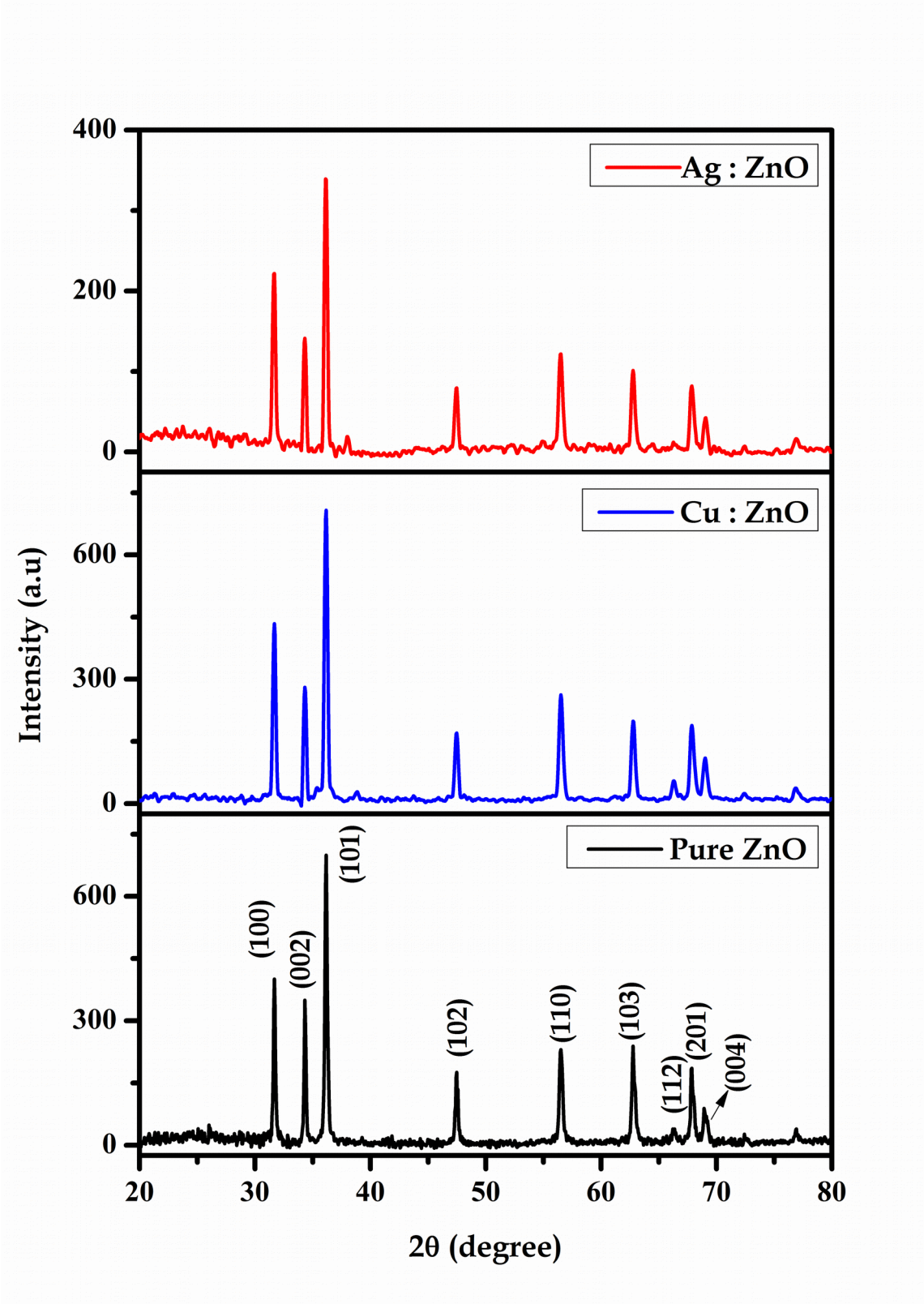

Figure 2

Preprint: C. Abinaya, M. Marikkannan, M. Manikandan, J. Mayandi, P. Suresh, V. Shanmugaiah, C. Ekstrum, J.M. Pearce, Structural and optical characterization and efficacy of hydrothermal synthesized Cu and Ag doped zinc oxide nanoplate bactericides. *Materials Chemistry and Physics* **184** (2016), pp. 172–182. http://dx.doi.org/10.1016/j.matchemphys.2016.09.039

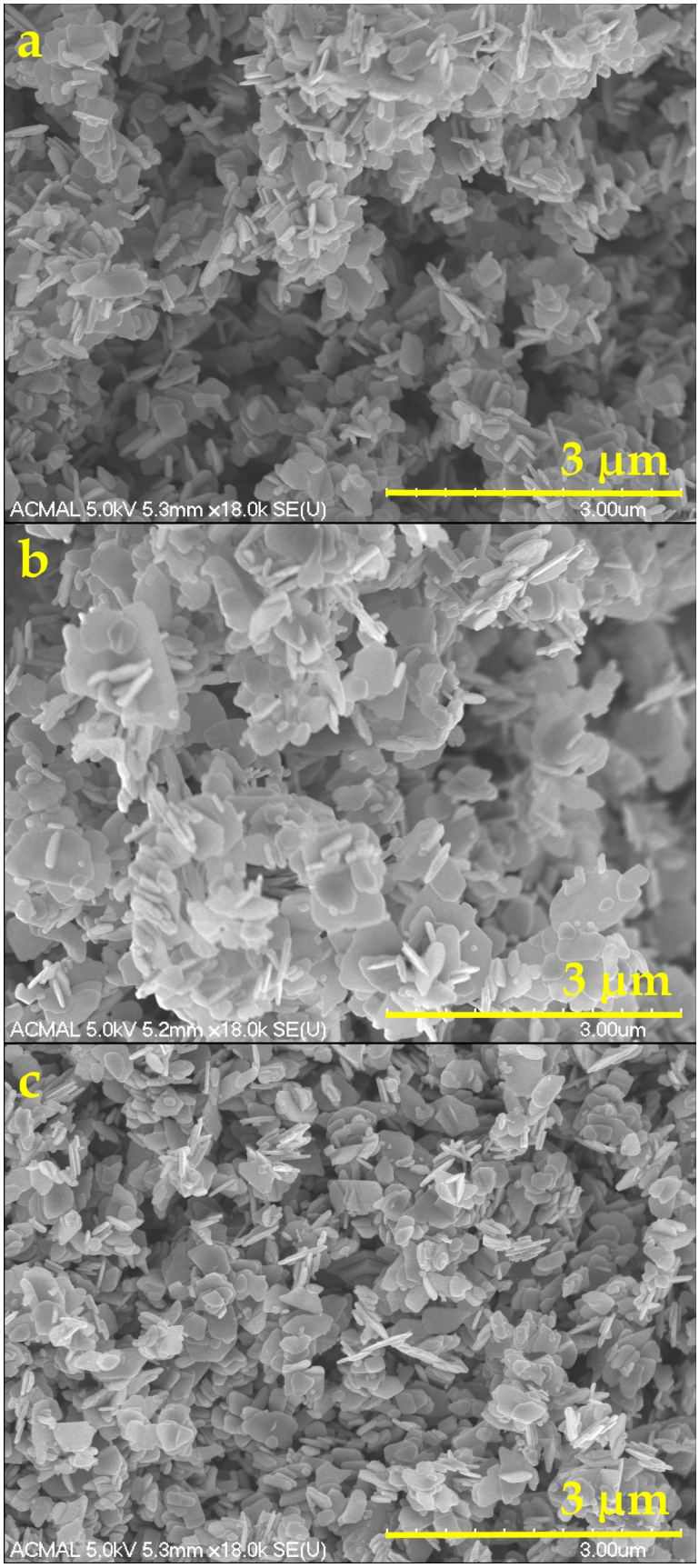

Preprint: C. Abinaya, M. Marikkannan, M. Manikandan, J. Mayandi, P. Suresh, V. Shanmugaiah, C. Ekstrum, J.M. Pearce, Structural and optical characterization and efficacy of hydrothermal synthesized Cu and Ag doped zinc oxide nanoplate bactericides. *Materials Chemistry and Physics* **184** (2016), pp. 172–182. http://dx.doi.org/10.1016/j.matchemphys.2016.09.039

Figure 3

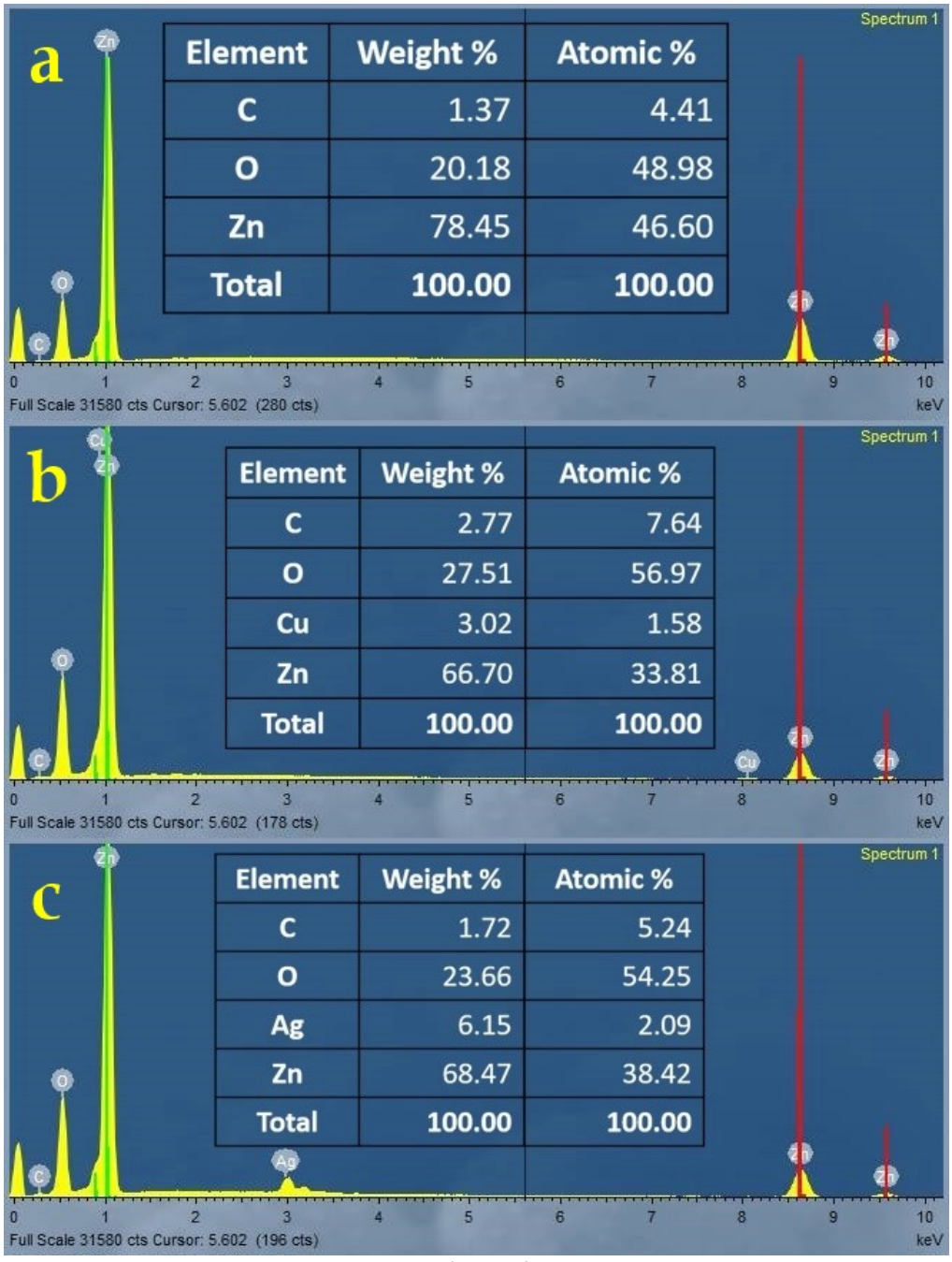

Figure 4

Preprint: C. Abinaya, M. Marikkannan, M. Manikandan, J. Mayandi, P. Suresh, V. Shanmugaiah, C. Ekstrum, J.M. Pearce, Structural and optical characterization and efficacy of hydrothermal synthesized Cu and Ag doped zinc oxide nanoplate bactericides. *Materials Chemistry and Physics* **184** (2016), pp. 172–182. http://dx.doi.org/10.1016/j.matchemphys.2016.09.039

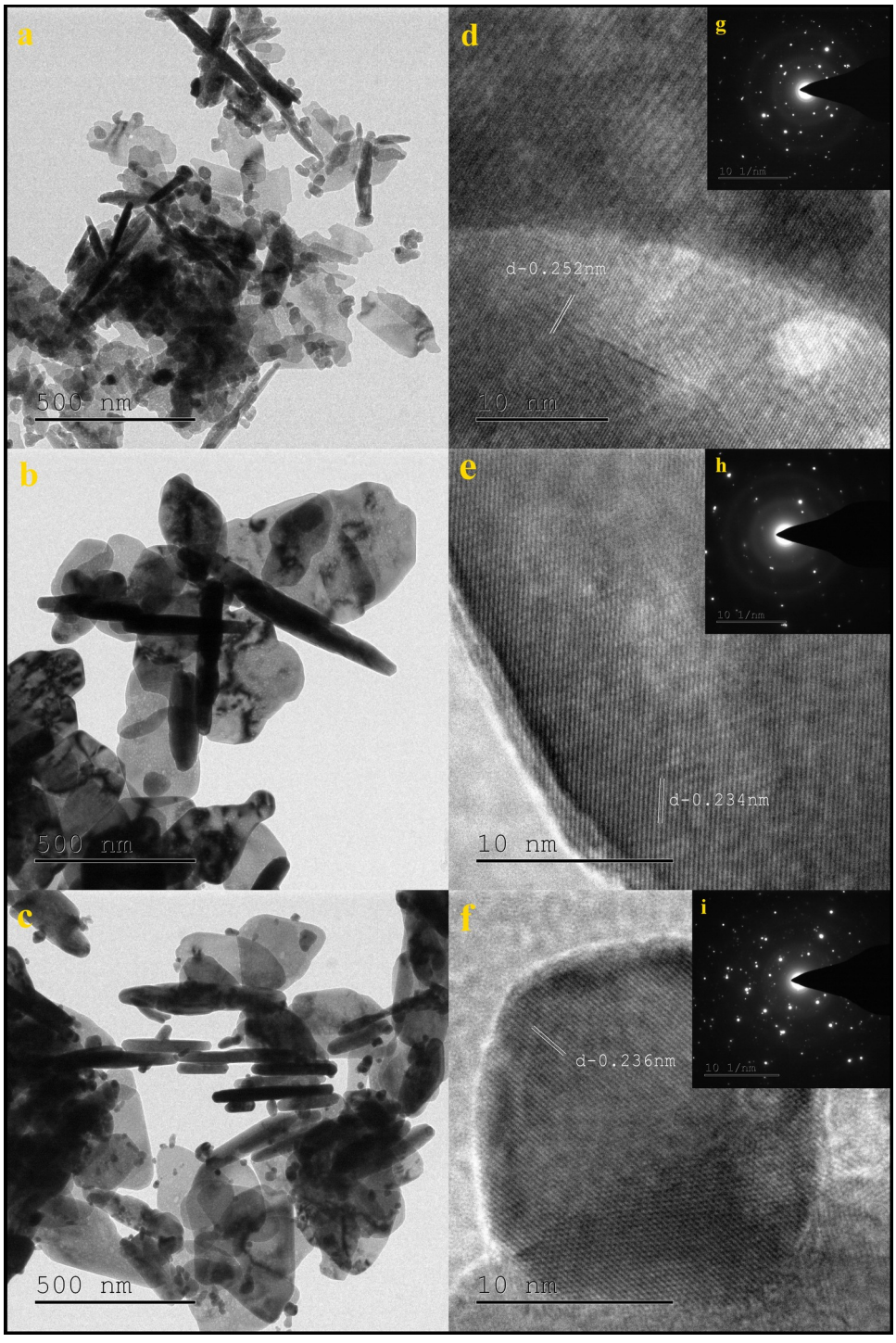

Figure 5

Preprint: C. Abinaya, M. Marikkannan, M. Manikandan, J. Mayandi, P. Suresh, V. Shanmugaiah, C. Ekstrum, J.M. Pearce, Structural and optical characterization and efficacy of hydrothermal synthesized Cu and Ag doped zinc oxide nanoplate bactericides. *Materials Chemistry and Physics* **184** (2016), pp. 172–182. http://dx.doi.org/10.1016/j.matchemphys.2016.09.039

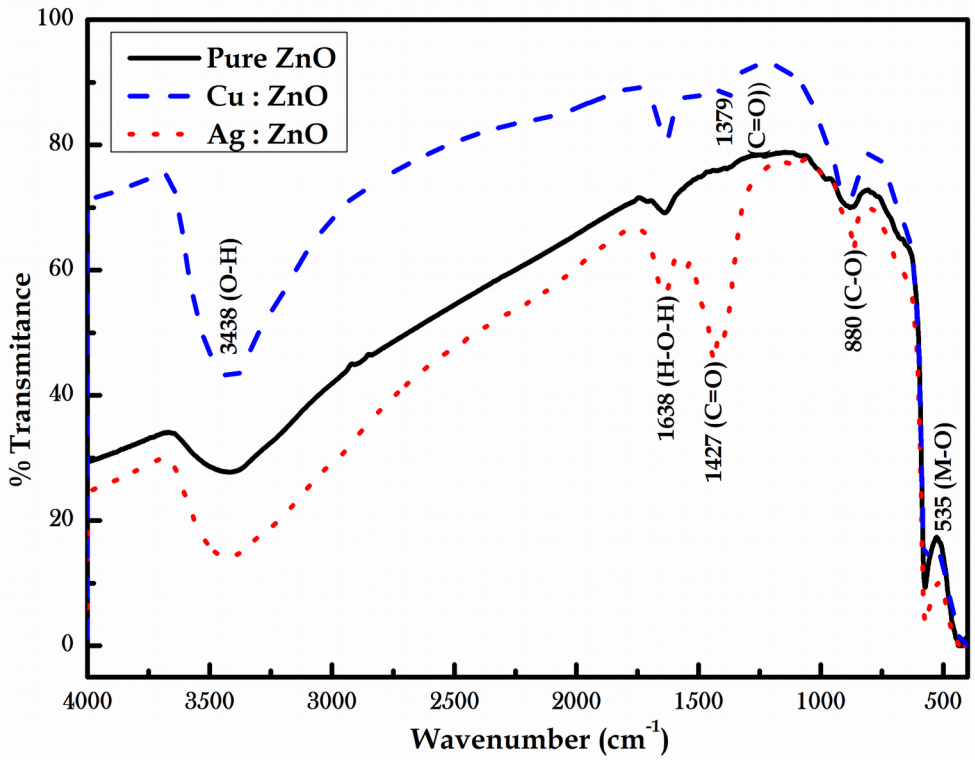

Figure 6

Preprint: C. Abinaya, M. Marikkannan, M. Manikandan, J. Mayandi, P. Suresh, V. Shanmugaiah, C. Ekstrum, J.M. Pearce, Structural and optical characterization and efficacy of hydrothermal synthesized Cu and Ag doped zinc oxide nanoplate bactericides. *Materials Chemistry and Physics* **184** (2016), pp. 172–182. http://dx.doi.org/10.1016/j.matchemphys.2016.09.039

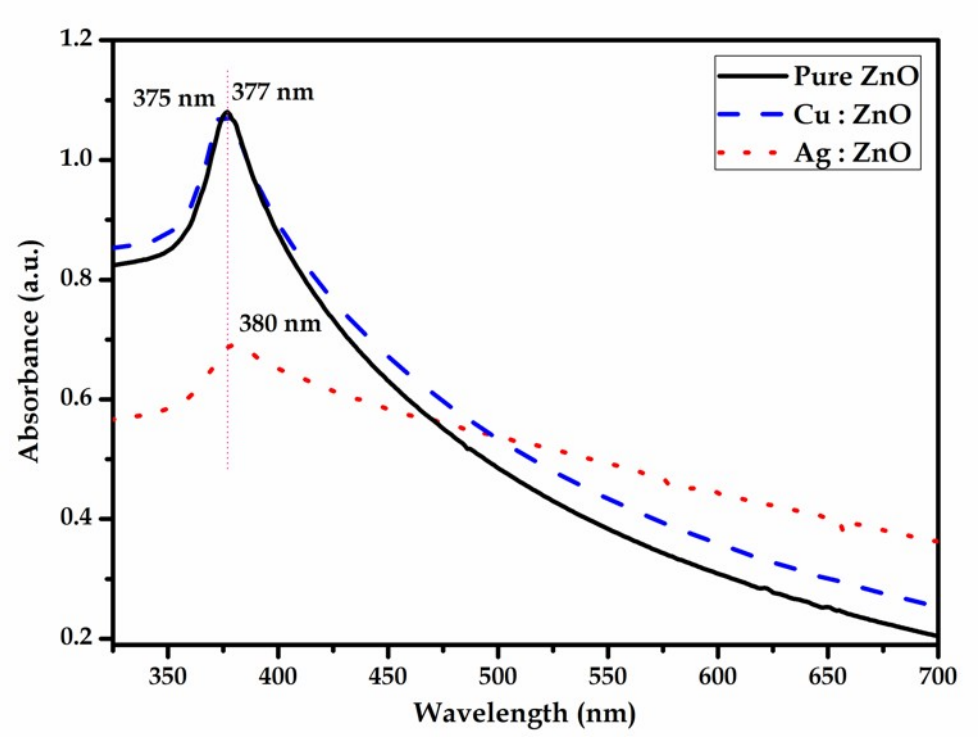

Figure 7

Preprint: C. Abinaya, M. Marikkannan, M. Manikandan, J. Mayandi, P. Suresh, V. Shanmugaiah, C. Ekstrum, J.M. Pearce, Structural and optical characterization and efficacy of hydrothermal synthesized Cu and Ag doped zinc oxide nanoplate bactericides. *Materials Chemistry and Physics* **184** (2016), pp. 172–182. http://dx.doi.org/10.1016/j.matchemphys.2016.09.039

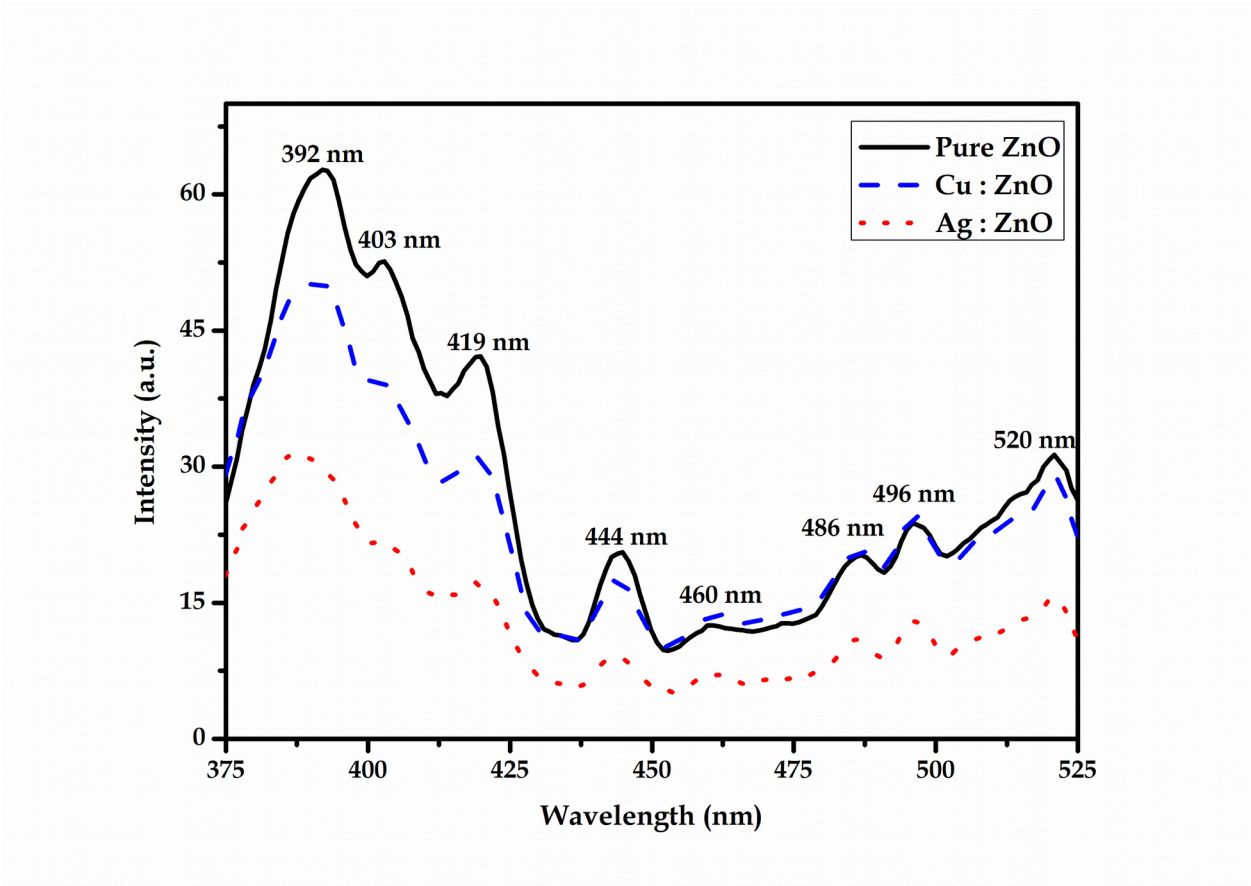

Figure 8

Preprint: C. Abinaya, M. Marikkannan, M. Manikandan, J. Mayandi, P. Suresh, V. Shanmugaiah, C. Ekstrum, J.M. Pearce, Structural and optical characterization and efficacy of hydrothermal synthesized Cu and Ag doped zinc oxide nanoplate bactericides. *Materials Chemistry and Physics* **184** (2016), pp. 172–182. http://dx.doi.org/10.1016/j.matchemphys.2016.09.039

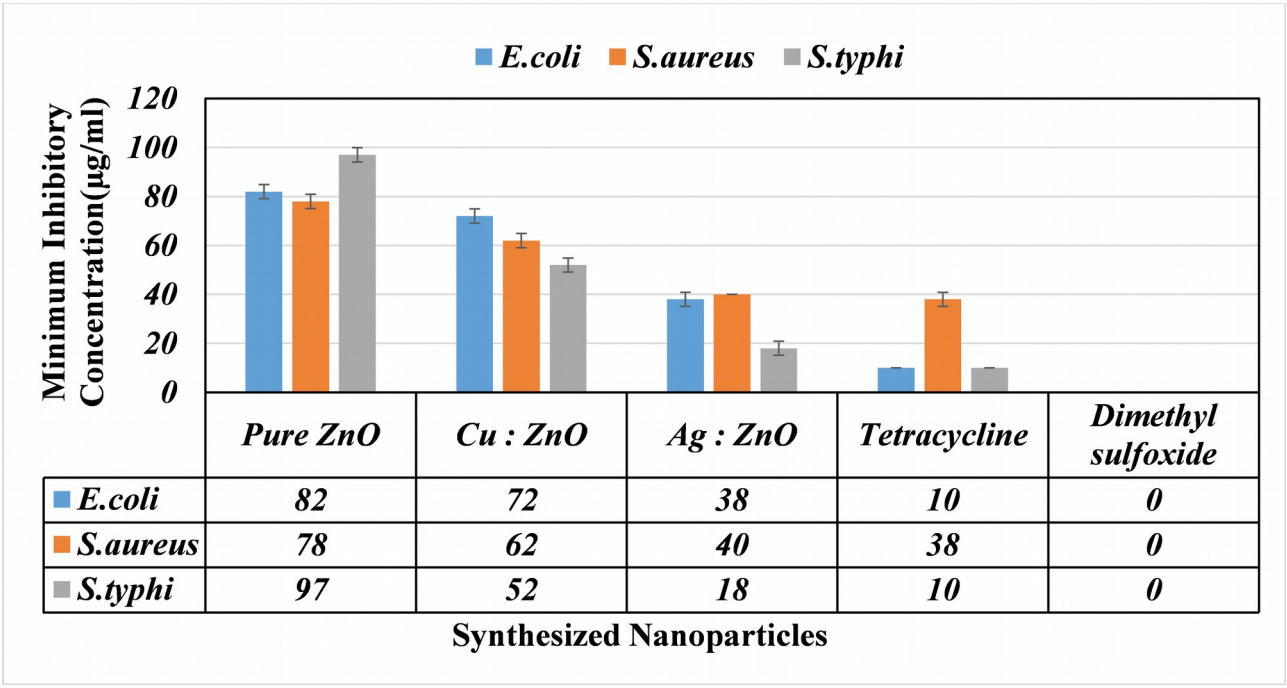

	Pure ZnO	Cu : ZnO	Ag : ZnO	Tetracycline	Dimethyl sulfoxide
E.coli	82	72	38	10	0
S.aureus	78	62	40	38	0
S.typhi	97	52	18	10	0

Figure 9